ELSEVIER

Physics of the Earth and Planetary Interiors 134 (2002) 213–237

PHYSICS OF THE EARTH AND PLANETARY INTERIORS

www.elsevier.com/locate/pepi

Magnetic stability and non-linear evolution of a selection of mean field dynamos

Paul Fotheringham, David Fearn*, Rainer Hollerbach

Department of Mathematics, University of Glasgow, Glasgow G12 8QW, UK

Received 29 March 2002; received in revised form 12 September 2002; accepted 16 September 2002

Abstract

The work presented herein is a continuation and extension of previous magnetic stability and non-linear evolution analyses by Hutcheson and Fearn [J. Fluid Mech. 291 (1995) 343; Phys. Earth Planet. Int. 97 (1996) 43; Phys. Earth Planet. Int. 99 (1997) 19]. The earlier works are based on imposed magnetic fields in cylindrical geometries which inevitably suffer from a certain degree of artificiality. We have therefore taken two important steps towards geophysical realism; firstly, our basic state field is now dynamically generated as part of a mean field dynamo mechanism, and secondly, we perform the analysis in a spherical shell with a finitely conducting inner core.

The analysis is undertaken numerically using a pseudo spectral time stepping procedure. This allows us to examine Ekman numbers as low as 2.5×10^{-4} whilst assuming that the Rossby number is identically zero. Our results indicate that magnetic instabilities, in the form of symmetry breaking bifurcations from the axisymmetric basic states supplied by the mean field dynamos, occur at Elsasser numbers of around O(10) or greater. Also, in each model, the symmetry breaking bifurcation was supercritical in nature. These results, although similar to the ones obtained in the previous cylindrical geometry work, hold when the basic state is oscillatory, a feature which was not explored in the studies mentioned above.
© 2002 Elsevier Science B.V. All rights reserved.

Keywords: Magnetic stability; Mean field dynamos; Bifurcations

1. Introduction

Typically the geomagnetic field is stable for relatively long periods of time ($\gtrsim 10^5$ years) but will reverse occasionally over a shorter timescale ($\lesssim 10^4$ years). Taking the basic state to represent the stable long-term field, the evolution of an instability of the field could be interpreted as one possible mechanism whereby the field reverses. This has been studied using a highly simplified model by Parker (1969) and Levy (1972) in the context of mean field dynamos. They envisaged a sudden change in the poloidal flow giving rise to reversal of toroidal field throughout the core, followed by the poloidal field. In particular, one would like to know if it is possible for the instability to evolve to a state with lower energy than at the critical point of stability. Furthermore, if one follows the non-linear evolution of an instability then one may gain insight into the reversal process of the geodynamo.

Magnetic stability analyses may provide upper bounds for the strength of the hidden toroidal component of the field by investigating the onset of instability of a given field configuration. Numerous studies have been made to ascertain this information. Many of these utilised the further simplification of a cylindrical model as opposed to the more realistic spherical geometry. This simplification was

* Corresponding author.
E-mail address: d.fearn@maths.gla.ac.uk (D. Fearn).

0031-9201/02/$ – see front matter © 2002 Elsevier Science B.V. All rights reserved.
PII: S0031-9201(02)00180-2

justified on the grounds that a rotating cylinder and a rotating sphere share some symmetries. Since our spherical study will extend the results of the previous cylindrical work we will now review the results to date.

The first numerical results to appear were from a series of linear studies by Fearn (1983, 1984, 1985, 1988) where a basic magnetic field was imposed, of the form

$$\boldsymbol{B}_0 = B_{\mathrm{M}} s F(s) \boldsymbol{e}_\phi \tag{1}$$

where s is the non-dimensionalised cylindrical radius. In magnetic stability analyses, the field is typically non-dimensionalised using a measure of the imposed field strength, here B_{M}. This introduces the Elsasser number to the non-dimensionalised momentum equation as the coefficient of the Lorentz force and is defined here as

$$\Lambda = \frac{B_{\mathrm{M}}^2}{\Omega \rho \mu_0 \eta}$$

where Ω is the mantle rotation rate, ρ the fluid density, μ_0 is the permeability of free space and η is the magnetic diffusivity of the fluid. The Elsasser number definition of Fearn included an extra factor of two in the denominator to that used here. The work of Fearn suggested that $\Lambda \geq \mathrm{O}(1)$ is a necessary condition for instability.

It is possible to define a more general version of the Elsasser number which more accurately represents the global variation of a given imposed field. We will define the energetic Elsasser number by

$$\Lambda' = \frac{(1/V) \int B^2 \, \mathrm{d}V}{\Omega \rho \mu_0 \eta} \tag{2}$$

where V is the volume of the computational domain.

In this work, we shall *not* impose an external field and instead use a mean field dynamo (with imposed α or α and ω) to generate an axisymmetric basic state. This has the advantage of being more realistic than an arbitrary imposed field but means we have to use an alternative non-dimensionalisation for $\boldsymbol{B}$ since its amplitude is not known in advance but emerges as part of the solution. We choose $\sqrt{\Omega \rho \mu_0 \eta}$ as our scale for $\boldsymbol{B}$. This means that Λ does not appear in our equations and is instead computed using the field strengths that emerge as part of the solution.

Note that we use the α-effect to generate only the axisymmetric part of the field. This is so that we can unambiguously investigate the effect of instability of the mean magnetic field. In the problem studied, the only source of non-axisymmetric components of $\boldsymbol{B}$ is instability of the mean field. Were we to introduce an α-effect into the non-axisymmetric part of the induction equation, we would introduce an alternative source for the non-axisymmetric part of $\boldsymbol{B}$.

Hutcheson and Fearn (1995) investigated the non-linear evolution of the instabilities of (1) for one particular choice of $F(s)$. They were able to achieve an Ekman number,

$$E = \frac{\nu}{\Omega \mathcal{L}^2}$$

where ν is the viscosity of the fluid and $\mathcal{L}$ a typical length scale of 4.5×10^{-3} using a spectral time-stepping code. Equilibrated non-linear solutions could only be found for $\Lambda > \Lambda_{\mathrm{c}}$, indicative of a supercritical bifurcation. The solution in the supercritical regime was dominated by the most unstable axially dependent mode from the linear analysis. The non-axisymmetric part took the form of an azimuthally drifting wave with a frequency similar to that of the most unstable mode.

Two later papers, Hutcheson and Fearn (1996, 1997), then investigated the influence of using a basic state depending also on z [$F = F(s, z)$], still with finite E. This allowed a more realistic dipole basic state to be considered as well as some more complicated quadrupole states. When the non-linear evolution of the linear instabilities was followed it was again discovered that the azimuthal symmetry breaking bifurcation was supercritical in nature regardless of the parity of the basic state. The first bifurcation was to a state with even azimuthal wavenumbers with dipole symmetry for the dipole state and quadrupole for the quadrupolar state. The dipole basic state had two subsequent bifurcations as Λ was increased, the effect of the symmetry breaking being to extract more energy from the basic state than before the bifurcation.

For $E = 0$ (the magnetostrophic approximation) Ogden and Fearn (1995) studied the effect of differential rotation on an imposed field with thermal buoyancy acting as well. They found if the differential rotation contained large enough regions of negative

shear ($\mathrm{d}\Omega_\mathrm{D}/\mathrm{d}s < 0$) then the effect of modest strength of differential rotation could be destabilising. This effect was most prominent for high Roberts number $q = \nu/\kappa$, where κ is the thermal diffusivity of the fluid. Fearn et al. (1997) and McLean (1997) then tried to isolate the effect that the differential rotation of the geostrophic flow might have on magnetic instabilities and to highlight potential differences with the finite E approach. By arbitrarily prescribing differential rotations $u_\phi = s\Omega_\mathrm{D}(s)$ in the linear onset problem it was confirmed that regions of negative shear were required to reduce the critical Elsasser number, Λ_c, for instability. It was also demonstrated that differential rotation could destabilise a field which was magnetically stable. In the non-linear regime (where the only non-linear effect considered was that of the geostrophic flow), various magnetically unstable field configurations were tried, with McLean (1997) including the realistic dipole field parity. For the s-dependent fields only those that concentrated field near to the inner core boundary produced subcritical bifurcations. With the addition of z-dependence virtually all the cases gave subcritical bifurcations.

The subcriticality of the magnetostrophic solutions was a direct consequence of the initial destabilising effect of the geostrophic flow, V_G. The viscous analyses showed only supercritical behaviour since other non-linear effects were dominant at the geophysically unrealistic value of E used. Both analyses were based on a cylindrical annulus model to enable a simplification of the governing equations, and indeed this would seem to be the "natural" geometry for the geostrophic flow since $V_\mathrm{G} = V_\mathrm{G}(s)$. However, in a cylindrical geometry, where the end walls are flat, one can show that $V_\mathrm{G} = V_\mathrm{G}(s, \phi)$. This shows that the geostrophic flow behaves in a fundamentally different way in the two geometries, and so it is desirable to remove this inconsistency. We wish to extend the cylindrical model results to the realistic spherical shell geometry, where V_G really is a function of s alone. We will be able to compare our results with the viscous studies of Hutcheson and Fearn and investigate whether subcriticality can exist in the spherical geometry at similar Ekman numbers to that used in the cylindrical analysis. We also hope to identify the role of differential rotation in our solutions and to examine how Λ varies with the forcing of the mean field generated basic state.

2. The model and governing equations

The system we have chosen to study consists of an electrically conducting fluid contained in a spherical shell. The region exterior to the fluid is taken as an electrical insulator to model the Earth's mantle. Of course, the mantle may, in fact, be weakly conducting but we shall ignore this fact in our present study as indeed most other models do. The region interior to the fluid (the inner core) is taken to be finitely conducting with the same electrical conductivity as the fluid itself. Neglecting inertial terms, the non-dimensional equations governing the evolution of the magnetic field $\boldsymbol{B}$ and fluid flow $\boldsymbol{u}$ are those shown below. In the outer core, we have

$$\frac{\partial \boldsymbol{B}}{\partial t} = \nabla \times (\boldsymbol{u} \times \boldsymbol{B} + \tilde{\alpha}\bar{\boldsymbol{B}}) + \nabla^2 \boldsymbol{B} \tag{3}$$

where $\bar{\boldsymbol{B}}$ denotes the axisymmetric part of $\boldsymbol{B}$

$$2\boldsymbol{e}_z \times \boldsymbol{u} - E\nabla^2 \boldsymbol{u} = -\nabla P + (\nabla \times \boldsymbol{B}) \times \boldsymbol{B} + \Theta(r, \theta)\,\boldsymbol{r} \tag{4}$$

where P is the pressure,

$$\nabla \cdot \boldsymbol{B} = 0, \qquad \nabla \cdot \boldsymbol{u} = 0 \tag{5}$$

and for the finitely conducting inner core

$$\frac{\partial \hat{\boldsymbol{B}}}{\partial t} = \nabla \times (\boldsymbol{u}_\mathrm{ic} \times \hat{\boldsymbol{B}}) + \nabla^2 \hat{\boldsymbol{B}} \tag{6}$$

where $\hat{\boldsymbol{B}}$ is the magnetic field in the inner core,

$$\nabla \cdot \hat{\boldsymbol{B}} = 0 \tag{7}$$

where $\boldsymbol{u}_\mathrm{ic} = \Omega_\mathrm{ic} r \sin\theta\, \boldsymbol{e}_\phi$. The inner core angular velocity, Ω_ic, is determined from the torque balance on the rigid inner core.

These equations have been non-dimensionalised using length $\mathcal{L} = r_\mathrm{o} - r_\mathrm{i}$ (where r_o is the outer-core radius and r_i is the inner-core radius), ohmic diffusion time $\mathcal{T} = \mathcal{L}^2/\eta$, speed $\mathcal{L}/\mathcal{T}$ and magnetic field strength $\mathcal{B} = \Omega\rho\mu_0\eta$.

The α-effect in the outer core is given by

$$\tilde{\alpha} = \alpha_0 \cos\theta \boldsymbol{e}_\phi \otimes \boldsymbol{e}_\phi \tag{8}$$

when there is an imposed buoyancy ($\Theta \neq 0$), and

$$\tilde{\alpha} = \alpha_0 \cos\theta \{\boldsymbol{e}_r \otimes \boldsymbol{e}_r + \boldsymbol{e}_\theta \otimes \boldsymbol{e}_\theta + \boldsymbol{e}_\phi \otimes \boldsymbol{e}_\phi\} \tag{9}$$

when there is is no buoyancy ($\Theta = 0$). In other words, when there is an imposed buoyancy, the form of the α-effect in (3) is $\tilde{\alpha}\bar{\boldsymbol{B}} = \alpha_0 \cos\theta \bar{B}_\phi \boldsymbol{e}_\phi$ while in the case of no imposed buoyancy, it is $\tilde{\alpha}\bar{\boldsymbol{B}} = \alpha_0 \cos\theta \bar{\boldsymbol{B}}$. These two cases correspond loosely with the notion of $\alpha\omega$ and α^2 dynamos, respectively. Although the terminology is technically incorrect, from now on the terms α^2 and $\alpha\omega$ will be used to distinguish the two cases. As in Hollerbach and Glatzmaier (1998) we give the buoyancy term the form

$$\Theta(r,\theta) = -\Theta_0 r \cos^2\theta$$

which results in an approximation to an ω-effect depending linearly on radius.

We have chosen to regenerate only the axisymmetric part of the field through $\tilde{\alpha}$ with the non-axisymmetric parts gaining energy only via the $\boldsymbol{u} \times \boldsymbol{B}$ term. Although the physically correct approach would be to include $\tilde{\alpha}$ in the entire field since the small scale helical motions should affect the field regardless of its azimuthal structure, one must bear in mind the point of this work. We are interested in improving the previously used diffusionless ambient states (imposed $\boldsymbol{B}_0$). We feel that by restricting $\tilde{\alpha}$ to only the axisymmetric part we have taken the problem one step further whilst retaining the underlying principles of a magnetic stability study. When non-axisymmetric solutions appear they can be unambiguously identified as arising from magnetic instability with no help from the non-axisymmetric part of $\tilde{\alpha}$. We will be able to examine how fully non-axisymmetric solutions equilibrate at supercritical forcings, a feature not previously studied in mean field models.

The flow is governed by the Navier–Stokes equation, (4), where we have neglected the inertial terms. The Rossby number for the Earth's core is small, possibly as low as $O(10^{-9})$. Including this term in a time-stepping calculation forces one into taking a small time-step to resolve the short timescales that may exist, even though one is only interested in the long-term behaviour, hence the use of the magnetic diffusion timescale as temporal normalisation. The magnetic field $\boldsymbol{B}$ has been non-dimensionalised with $\sqrt{\Omega\rho\mu_0\eta}$ as discussed previously.

We do not make the full magnetostrophic assumption by neglecting the viscous term as well. Despite geophysically relevant values of E being perhaps as low as $O(10^{-15})$ (a typical estimate of the viscosity in the core is of the order of $\nu = 10^{-6}\,\mathrm{m^2\,s^{-1}}$, see for example, Alfe et al., 2000), we chose to retain this as a parameter to circumvent any discontinuities on the tangent cylinder via shear layers. Correcting for the differences in their definition of E, the lowest Ekman number of the Hutcheson and Fearn works was 4.5×10^{-4} while for our α^2 dynamo we have managed 2.5×10^{-4}. For details of the boundary conditions and the numerical method, see Hollerbach (2000). In Section 3, we begin with the α^2 dynamo and move onto the $\alpha\omega$ dynamo in Sections 4–6 for three different non-zero values of Θ_0. Each section follows the same pattern. Firstly, the purely axisymmetric results are outlined, i.e. the basic state information. Secondly, a non-axisymmetric linear stability analysis is carried out on the axisymmetric states and thirdly, full non-linear non-axisymmetric results are presented.

3. $\Theta_0 = 0$ (α^2 dynamos)

3.1. Axisymmetric results

The axisymmetric problem has already received some attention from Hollerbach and Jones (1993). Using the form of $\tilde{\alpha}$ in (9) and $E = 2.5 \times 10^{-4}$ they studied dipole constrained solutions up to $\alpha_0 = 8.0$. In our present study we shall attempt to find where the axisymmetric field becomes unstable to non-axisymmetric perturbations or indeed perturbations of the opposite parity. From the outset then, we will allow for quadrupole symmetry. Also, it will turn out that the axisymmetric state becomes unstable at much higher values of α_0 than previously studied and so we have chosen to retain an Ekman number of 2.5×10^{-4}. Given that we will be running fully 3D calculations later on (see Section 3.3) it would be unwise to try to reduce E any further with current computational resources. The critical values of α_0 for the linear onset of dynamo action are quoted in Table 1. The value of α_c for the dipole mode is in exact agreement with that of Hollerbach and Jones.

To map out the bifurcation sequence the value of α_0 was increased in steps of 0.5 and the system was

Table 1
The linear onset value, α_c, for dynamo action when $\Theta_0 = 0$

	Dipole	Quadrupole
α_c	5.15	5.23

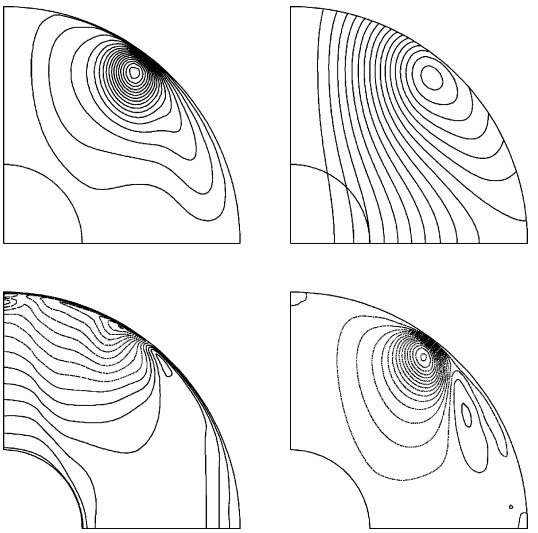

Fig. 1. Contour plots of B, $Ar\sin\theta$ (top row) and $v/r\sin\theta$, $\psi r\sin\theta$ (bottom row) at $\alpha_0 = 14.0$, $\Theta_0 = 0$. Contour intervals are 0.2, 0.08, 5 and 0.08, respectively.

allowed to equilibrate at each stage. The dipole branch was followed to $\alpha_0 = 17.0$ and was found to be steady and stable to quadrupole perturbations. A pure parity quadrupole branch was found to co-exist in the region $5.5 \lesssim \alpha_0 \lesssim 7.0$. This branch was also steady and stable to perturbations of the opposite symmetry. At $\alpha_0 = 5.5/7.0$, it gains/loses stability, presumably through a pitchfork bifurcation.

The structure of the dipolar solutions in this regime are shown in Fig. 1 for $\alpha_0 = 14.0$. The toroidal field is very localised adjacent to the outer boundary and close to the maximum of the poloidal field. The meridional flow shows similar behaviour. The angular velocity of the fluid has some locally geostrophic flow appearing in the region outside the tangent cylinder. There is just as much super-rotation as there is sub-rotation, with the interface between the two passing very close to the maxima in the other quantities. Inside the tangent cylinder, there are the beginnings of the formation of a shear layer almost parallel to the rotation axis but otherwise the flow simply accommodates the super-rotation of the inner core.

To be sure that this is a genuine feature and not a numerical artifact we chose this value of α_0 to carry out a truncation test. (Actually, this value was also chosen because, as we shall see in the next section, the field has already become unstable to non-axisymmetric perturbations at this point.) As truncation levels were increased the magnetic energy of the solution tended towards a constant limit. By altering the individual truncation limits and comparing the magnetic energy to the limiting value the most CPU efficient truncations were found to consist of 34 Chebyshev polynomials in radius and 40 Legendre functions in θ for *both* field and flow. All the work presented in this section, including the non-axisymmetric results to follow, used this truncation and were time-stepped with $\Delta t = 2\times10^{-5}$ (recall that time is non-dimensionalised using the ohmic diffusion time). Tests were undertaken to ensure this time step was adequate to ensure accuracy.

3.2. Linear stability results

We now turn to the topic of primary interest in this study. Given a steady state axisymmetric solution $(\boldsymbol{B}_0, \boldsymbol{u}_0)$ we can split each of the field and flow into two parts,

$$\boldsymbol{B} = \boldsymbol{B}_0 + \boldsymbol{b}_m, \qquad \boldsymbol{u} = \boldsymbol{u}_0 + \boldsymbol{u}_m \tag{10}$$

where $\boldsymbol{b}_m$ and $\boldsymbol{u}_m$ represent the non-axisymmetric components with particular azimuthal wavenumber m. The linearised versions of Eqs. (3) and (4) then become

$$\frac{\partial \boldsymbol{b}_m}{\partial t} = \nabla\times(\boldsymbol{u}_0\times\boldsymbol{b}_m + \boldsymbol{u}_m\times\boldsymbol{B}_0) + \nabla^2\boldsymbol{b}_m \tag{11a}$$

$$2\boldsymbol{e}_z\times\boldsymbol{u}_m = E\nabla^2\boldsymbol{u}_m + (\nabla\times\boldsymbol{B}_0)\times\boldsymbol{b}_m + (\nabla\times\boldsymbol{b}_m)\times\boldsymbol{B}_0 - \nabla P_m \tag{11b}$$

At this point, we will introduce some notation to describe the parities of our solutions. If a vector quantity, $\boldsymbol{S}$, is dipolar then we will denote this by $\boldsymbol{S}\in\mathcal{D}$ and if it is quadrupolar we will say $\boldsymbol{S}\in\mathcal{Q}$. The symmetries described by the terms dipole and quadrupole have the following interpretation when $\boldsymbol{S}$ is expressed in spherical polar coordinates:

$$\begin{array}{ll} \text{dipole} & \text{quadrupole} \\ S_r(r,\pi-\theta,\phi) = -S_r(r,\theta,\phi), & S_r(r,\pi-\theta,\phi) = S_r(r,\theta,\phi), \\ S_\theta(r,\pi-\theta,\phi) = S_\theta(r,\theta,\phi), & S_\theta(r,\pi-\theta,\phi) = -S_\theta(r,\theta,\phi), \\ S_\phi(r,\pi-\theta,\phi) = -S_\phi(r,\theta,\phi), & S_\phi(r,\pi-\theta,\phi) = S_\phi(r,\theta,\phi). \end{array} \tag{12}$$

From Eqs. (11a) and (11b) one can easily enough verify the possible symmetries that are permitted for pure parity basic states. One can either have

$$\boldsymbol{b}_m \in \mathcal{D}, \quad \boldsymbol{u}_m \in \mathcal{Q} \quad \text{or} \quad \boldsymbol{b}_m \in \mathcal{Q}, \quad \boldsymbol{u}_m \in \mathcal{D} \quad \text{when} \quad \boldsymbol{B}_0 \in \mathcal{D} \tag{13}$$

or

$$\boldsymbol{b}_m \in \mathcal{D}, \quad \boldsymbol{u}_m \in \mathcal{D} \quad \text{or} \quad \boldsymbol{b}_m \in \mathcal{Q}, \quad \boldsymbol{u}_m \in \mathcal{Q} \quad \text{when} \quad \boldsymbol{B}_0 \in \mathcal{Q} \tag{14}$$

Let us first discuss the short branch of quadrupolar solutions since these turn out to be of little interest. By testing the linear stability of the $\alpha_0 = 7.0$ state for values of the azimuthal wavenumber m from 1 to 8 it was concluded that this branch was stable to all perturbations. Indeed, the decay rates associated with each mode were large enough to deduce that for these field strengths there was no danger of non-axisymmetric instability at all. The form of the linear eigenfunctions was that of a steady drift about the rotation axis as they decayed.

Turning now to the more interesting dipole case, we first note that an α^2 dynamo is useful in that it has allowed us to test the stability of steady states. Since our basic state is trying to model the long-term geomagnetic field, this is one advantage the model has over the $\alpha\omega$ dynamo, despite being in the weak field regime. When tested at $\alpha_0 = 8.0$, the dipole solution was found to be stable with respect to non-axisymmetric perturbations up to $m = 8$. Indeed, it was not until $\alpha_0 \sim 13.0$ that any instability was found. Table 2 shows the values of α_0 at which the various non-axisymmetric modes begin to go unstable, and to which parity of field.

The first surprising thing to note, given the rather high value of $E = 2.5 \times 10^{-4}$ is that the mode with the largest structure in azimuth, i.e. $m = 1$ is not excited first and indeed is not excited in the range of α_0 tested.

Table 2
The critical values of α_0 and parities for the linear onset of non-axisymmetric modes of azimuthal wavenumber m

α_0	m	Parity
13.1	3	$\mathcal{D}$
13.4	2	$\mathcal{D}$
14.1	4	$\mathcal{D}$

An $m = 2$ mode is, however, the second mode excited at a value of α_0 very close to the $m = 3$ critical value. A common feature of all these modes is their dipole parity.

We can now make our first comparisons with the results of the studies of Hutcheson and Fearn (hereafter collectively referred to as HF). In their analysis, the first mode to go unstable was $m = 1$ when the basic state was independent of z, i.e. quadrupole. This was at an Ekman number more than 10 times our value which may explain the discrepancy. When they introduced a z-dependence they also lowered their Ekman number to a value comparable to ours. At this value, both dipole and quadrupole basic states yielded an $m = 2$ mode as the first instability which suggests that for $E \sim 10^{-4}$ one should perhaps not expect to see an $m = 1$ mode coming in first after all.

The other similarity between the two models is the preference for a dipole symmetry perturbation when the basic state is dipolar. Indeed, HF also found that for their quadrupole state the preferred perturbation field parity was quadrupole, suggesting at first glance that the controlling influence is the parity of the field. However, on closer inspection, we see that for both cases the perturbations have a quadrupole flow (see Eqs. (13) and (14)) which is the parity required for the formation of columnar rolls, a common feature of non-magnetic convection and which suggests that the Taylor-Proudman theorem may still be partially operating. For our solutions, the preferred parity could also be tied in to the existing parity of the quadrupolar basic state flow. Even though our quadrupole basic state was not linearly unstable, a comparison of the decay rates between $\mathcal{D}$ and $\mathcal{Q}$ perturbations showed that the dipole perturbations were damped much more strongly than their quadrupole counterparts.

At $\alpha_0 = 13.1$, the Elsasser number, $\Lambda = 28.3$, which is one order of magnitude different from the (converted) value of 3.34 found by HF for their dipole basic state (the value for the quadrupole was 4.12). As noted before, the field has localised very strongly near the outer boundary and at a preferred latitude and so the classical Elsasser number, which only provides information about the maximum of the field, does not give a very accurate picture of the field structure. In contrast, we find the value of Λ' to be 4.53 which is in much better agreement with HF's value. The field

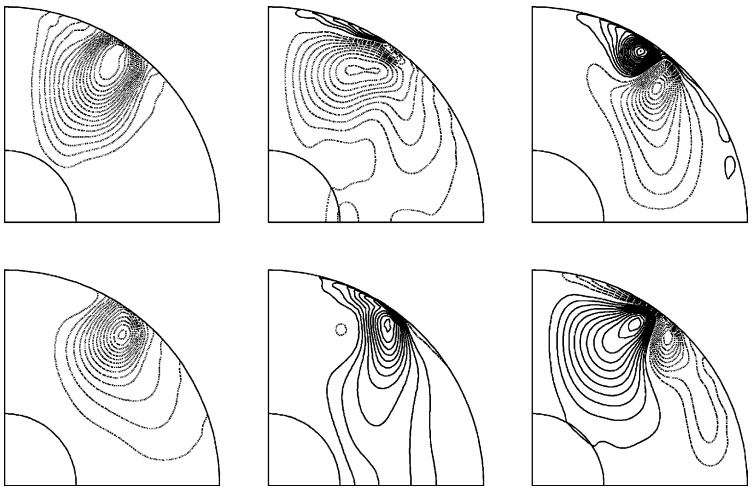

Fig. 2. Contour plots of the linear eigenfunction of the $m = 3$, dipole mode at $\alpha_0 = 14.0$, $\Theta_0 = 0$. Top row shows the meridional structure of the r, θ, ϕ components of $\boldsymbol{b}$ at an arbitrary phase. Bottom row shows the same but with 90° greater phase angle. For the sake of comparison, all three components are shown at the same contour interval.

structure in HF is much more uniform and hence Λ is probably an adequate measure of the field strength in that case.

Finally, we turn to the structures of the non-axisymmetric eigenfunctions. Fig. 2 shows the three components of the $m = 3$ dipole magnetic field at the supercritical value $\alpha_0 = 14.0$. The top row represents the r, θ structure at an arbitrary point in time and azimuth. The lower row shows the same but phase-shifted 90°, i.e. either 90° round in ϕ, a quarter revolution backwards in time, or a suitable shift in both. It is immediately clear that the instability has formed at the same latitude and radius at which the basic state concentrates. This is not unexpected and is in agreement with the solutions found by HF.

3.3. Fully 3D results

We now solve the full system given by (3)–(7), recalling that the α-effect only regenerates the axisymmetric field, calculating the interactions of all the azimuthal modes with one another up to our truncation limits, MB and MU (MB is the number of azimuthal modes in the expansion for the magnetic field and *MU* the number for the flow). In practice, we always took MB = MU which seems to be the most reasonable choice. We chose MB = 9 and started the run at the supercritical value of $\alpha_0 = 14.0$. The axisymmetric basic state was used as the initial condition for the $m = 0$ part but we chose to include finite energy in both $m = 2$ and $m = 3$ since both of these were linearly unstable for this choice of α_0. The corresponding linear dipolar eigenfunctions were fed in and normalised so that each had one tenth of the energy of the $m = 0$ part.

As the run progressed the behaviour of the two non-axisymmetric modes was quite different. The $m = 2$ mode started to decay immediately whilst the $m = 3$ mode settled into a finite amplitude equilibration. There was no growth observed in any of the other modes except the $m = 6$ and $m = 9$ dipole parities where the quadratic interaction of $m = 3$ with itself generated a finite amplitude solution. The run was continued until all non-zero modes had equilibrated to their final state. The $m = 0$ mode was still steady whereas $m = 3, 6$ and 9 took the form of azimuthally drifting waves. This equilibration can be thought of as steady in the sense that the energy associated with it is constant. The equilibrated energies for the non-zero modes are shown in Table 3.

Note that the axisymmetric magnetic energy has changed by only 3% from its original value of 38.2. Most of this energy is in the $m = 3$ mode but clearly the instability is unable to extract much energy from

Table 3
Magnetic energies for the non-zero azimuthal modes at $\alpha_0 = 14.0$

m	0	3	6	9
E_M	37.1	9.38×10^{-1}	8.84×10^{-3}	1.99×10^{-4}

the basic state. Subsequently, there was no change in the structures of the axisymmetric and $m = 3$ parts from Figs. 1 and 2. A view of the azimuthal structure of B_ϕ and u_ϕ is shown in Fig. 3 in the plane $z = 1$. The $m = 3$ mode has enough energy to produce a clear perturbation to the underlying axisymmetric contours, however, despite the inclusion of the $m = 6$ and 9 modes, there is no evidence of them whatsoever in the plots.

We now turn to the question of subcriticality and test if our full non-axisymmetric solution can exist in the region of linear stability, $\alpha_0 \lesssim 13.1$. Using an equilibrated solution at $\alpha_0 = 13.25$ (same properties as above) as an initial condition, a run at $\alpha_0 = 13.05$ was attempted. It was immediately clear that all the non-axisymmetric parts were decaying, leaving behind the $m = 0$ steady state. This suggests that the azimuthal symmetry breaking bifurcation is supercritical in nature. We can, of course, test for this up to arbitrary precision by taking values of α_0 which are closer and closer to the linear onset value but this is not necessary. In the context of geomagnetic field reversals, we are more interested in a solution which can equilibrate at a reasonable strength below linear onset than one which can exist just barely below onset. In the former case, a small perturbation of the axisymmetric solution close to linear onset would result in the system jumping to a finite amplitude instability. One possibility is that such a jump could trigger a reversal.

Table 4
Magnetic energies for the purely axisymmetric solution $(E_M)^*_{m=0}$, the $m = 0$ part of the full non-axisymmetric solution $(E_M)_{m=0}$, and the total energy of the full solution $(E_M)_{Total}$ for three values of α_0

α_0	$(E_M)^*_{m=0}$	$(E_M)_{m=0}$	$(E_M)_{Total}$
13.25	33.1	32.9	33.0
14.0	38.2	37.1	38.0
16.0	52.1	47.9	51.7

Comparing our results to the cylindrical analysis of HF we can confirm that the non-axisymmetric solution is dominated by the most unstable mode from the linear analysis. Furthermore, the initial azimuthal breaking bifurcation is of a supercritical nature.

We can now increase α_0 to see if any subsequent bifurcations are subcritical. The non-axisymmetric solution that we have can be thought of as steady and so, in addition to the axisymmetric state that we have just looked at, is another possible candidate to simulate the long-term field. One should note, however, that the truncation tests suggest $\alpha_0 = 14.0$ is just within the limits of resolution and so the following results must be interpreted with that in mind.

Increasing α_0 in steps of 0.5 from 14.0, the solution remained as before up to $\alpha_0 = 16.0$. Table 4 lists the magnetic energies associated with the axisymmetric field before and after the addition of other azimuthal modes as well as the total energy of the full non-axisymmetric solution at three different values of

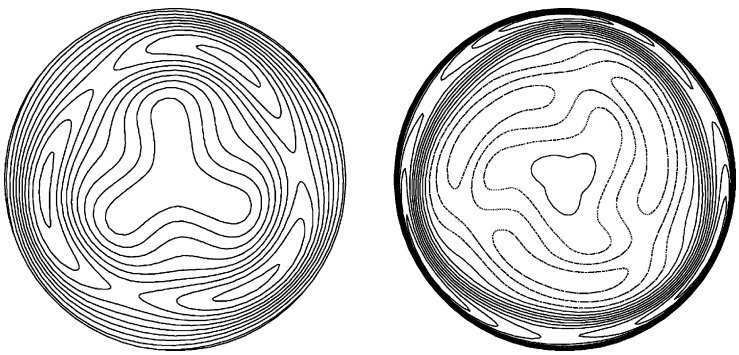

Fig. 3. Contour plots of the full non-axisymmetric solution at $\alpha_0 = 14.0$, $\Theta_0 = 0$, taken through the slice $z = 1$. On the left is B_ϕ with a contour interval of 0.35. On the right is u_ϕ with a contour interval of 2.5.

α_0. One can see that in each case the energy in the axisymmetric part of the full solution has been decreased from its original (purely axisymmetric) value since the non-axisymmetric modes are drawing their energy from the basic state. The total magnetic energy of the non-axisymmetric state is very similar to the original $m = 0$ value near the azimuthal symmetry breaking bifurcation as one would expect. This is followed by an increasing difference as α_0 is increased with the total energy always less than the original axisymmetric magnetic energy.

At $\alpha_0 = 16.5$, a change in the temporal behaviour was observed but no new azimuthal modes were excited. The drifting waves acquired a superimposed oscillation as they rotated and the axisymmetric part also became oscillatory. The frequency of oscillation for each azimuthal mode was higher than the drift frequency, but did not appear to be commensurate with it, resulting in a quasi-periodic solution. This new state was tested for subcriticality by reducing α_0 to 16.0, but again, a return to the original steady drift behaviour was observed.

At $\alpha_0 = 17.0$, yet another bifurcation was observed, this time another azimuthal symmetry breaking accompanied by another change in the temporal behaviour. Now all azimuthal modes were being excited from $m = 1$ through to our top limit of $m = 9$ but again the only symmetry present in the system was dipolar. The vacillating drift of the non-axisymmetric components seemed to adopt yet another superimposed frequency but we did not run the solution long enough to track down this detail. At this point, the non-axisymmetric modes started having an impact on the axisymmetric part. Table 5 shows the energy in each azimuthal mode at a random snapshot in time.

Table 5
Magnetic energies for each azimuthal mode at $\alpha_0 = 17.0$

m	E_M
0	48.5
1	9.82×10^{-2}
2	6.12×10^{-2}
3	6.24
4	4.52×10^{-2}
5	7.66×10^{-3}
6	0.251
7	5.88×10^{-3}
8	1.16×10^{-3}
9	2.76×10^{-2}

The $m = 3$ mode and its harmonics have increased more than the axisymmetric part whilst the other modes are also becoming important with $m = 1$, 2 and 4 containing more energy than the $m = 9$ mode. This bifurcation, however, turned out to be supercritical leaving us with no subcritical bifurcations in our α^2 model at all.

In brief summary, we have confirmed that the onset of instability of an axisymmetric basic state occurs at around $\Lambda' \sim O(1)$ ($\Lambda \sim O(10)$ for a localised field) in our α^2 model. The evolution of the initial instability is governed by the most unstable linear mode and equilibrates in a state almost unchanged from the initial configuration. All bifurcations have tested negative for subcriticality, although one cannot have full confidence in the secondary and tertiary bifurcations due to limited resolution. The next sections examine how these results carry through to the strong-field regime pertinent to a dynamo of type $\alpha\omega$.

4. $\Theta_0 = 200$ ($\alpha\omega$ dynamo)

4.1. Axisymmetric results

The present choice of Θ_0 is that used by Hollerbach and Glatzmaier (1998), hereafter referred to as HG. Note that HG used a numerical code developed by Glatzmaier independently of the Hollerbach code on which the current work is based. Confirmation of their results therefore increases confidence in our own code. We increase the Ekman number from that used in the previous section to 5×10^{-4} which allows exact comparison with HG. In Table 6 we report our own findings for α_c as well as the approximate values from previous studies. The agreement is clearly satisfactory.

Table 6
The linear onset value, α_c, for dynamo action when $\Theta_0 = 200$

	Dipole	Quadrupole
α_c	8.0	6.3
	~8	~6

The second row indicates approximate values from previous studies.

In the non-linear regime, the initial bifurcation is to a pure quadrupole state which oscillates about a zero time average and is dominated by dynamo waves travelling from the equator to the pole. We were able to reproduce their plots of the solution at $\alpha_0 = 10.0$. HG reported a symmetry breaking bifurcation at $\alpha_0 \sim 11$, after which the quadrupole parts continued to oscillate about a zero mean with the now excited dipole parts oscillating about a non-zero mean. The period of the quadrupole parts was double that of the dipole parts which suggested the quadrupole parts consisted of only the odd harmonics with the dipole having the even (including zero) harmonics. They went on to plot this solution at $\alpha_0 = 15$. We are able to reproduce this.

However, the details of the bifurcation sequence to get from the pure parity state to the mixed parity state are not as straightforward as originally proposed. It turns out that the transition is actually accommodated by, not one, but *four* distinct bifurcations. Since they are not strictly relevant to the non-axisymmetric linear stability analysis we will do later (all these states turn out to be stable to non-axisymmetric perturbations), we shall only briefly summarise the short sequence of bifurcations.

The first bifurcation actually occurs at $\alpha_0 = 10.2$ and is indeed a symmetry breaking bifurcation in that the dipole parts are now excited and oscillate about a zero mean. They have the same period as the quadrupoles with only odd harmonics present at this point. At $\alpha_0 = 10.8$ the second bifurcation takes place and breaks the odd harmonic symmetry in the temporal behaviour. Now all harmonics are present and both quadrupole and dipole parts oscillate about a non-zero mean. If one then progresses to $\alpha_0 = 11.4$ the solution exhibits two completely disparate timescales. There is a short timescale that corresponds to the period of oscillation of the solution before the bifurcation and a much longer timescale over which the dipole part of the solution changes sign.

The quasi-periodic behaviour is ended at a bifurcation at $\alpha_0 = 11.8$. Beyond this point, we return to the solution branch described by HG which is the one of most interest in the following sections. This branch is a periodic mixed parity state with even harmonics in time for the dipoles and odd for quadrupoles. HG quote that this branch goes unstable around $\alpha_0 \sim 30$ but do not give any further details. We find there is a transition to chaotic behaviour at the smaller value of $\alpha_0 = 25$. This discrepancy is slightly worrying, but it is quite conceivable that HG did not take particularly small steps in α_0 in this regime since they were more interested in getting the strong field branch which exists for even higher α_0. Indeed, we were able to reproduce the strong field branch, which comes in at $\alpha_0 = 42$ in the form of a steady mixed parity solution. The fact that we have successfully reproduced all the contour plots from HG suggests our code is working satisfactorily and that any discrepancies are simply due to a lack of resolution in α_0 in HG.

We did not search for solution branches coexisting with the pure quadrupole and mixed branches at the lower end of the bifurcation sequence. If they exist, there is nothing to suggest that they should behave any differently, unless they have radically different field morphologies or magnetic energies, neither of which seems likely.

We conclude this section on the purely axisymmetric behaviour of our model by showing an example of the solution at $\alpha_0 = 14.0$. The contour plots can be seen in Fig. 4 which, due to the oscillatory nature of the solution, shows six evenly spaced snapshots throughout one period. The equatorial symmetry is clearly broken at any instant in time, however, as pointed out by HG, one can recover an equatorial symmetry by comparing plots half a period apart.

The convergence of all the results in the range $6.3 \leq \alpha_0 < 25$ were checked by performing a truncation test at $\alpha_0 = 20.0$. Since the Ekman number has been doubled from the last chapter, it was found that truncations consisting of 26 Chebyshev polynomials and 32 Legendre functions were adequate to produce the period-averaged magnetic energy to an accuracy of better than 0.5%. In fact, to facilitate a more thorough exploration of the detailed bifurcation sequence, recalling the long period of the heteroclinic connection, values of α_0 less than or equal to 15.0 were found using 22 Chebyshev polynomials and 28 Legendre functions which seemed to produce satisfactory results. The runs in both the chaotic and strong field branches were performed at the 26, 32 level and so must be treated with caution. However, the strong field branch was exactly as found in HG and so the results are better than just qualitatively correct. As before, the same truncations were carried through to the non-axisymmetric analyses.

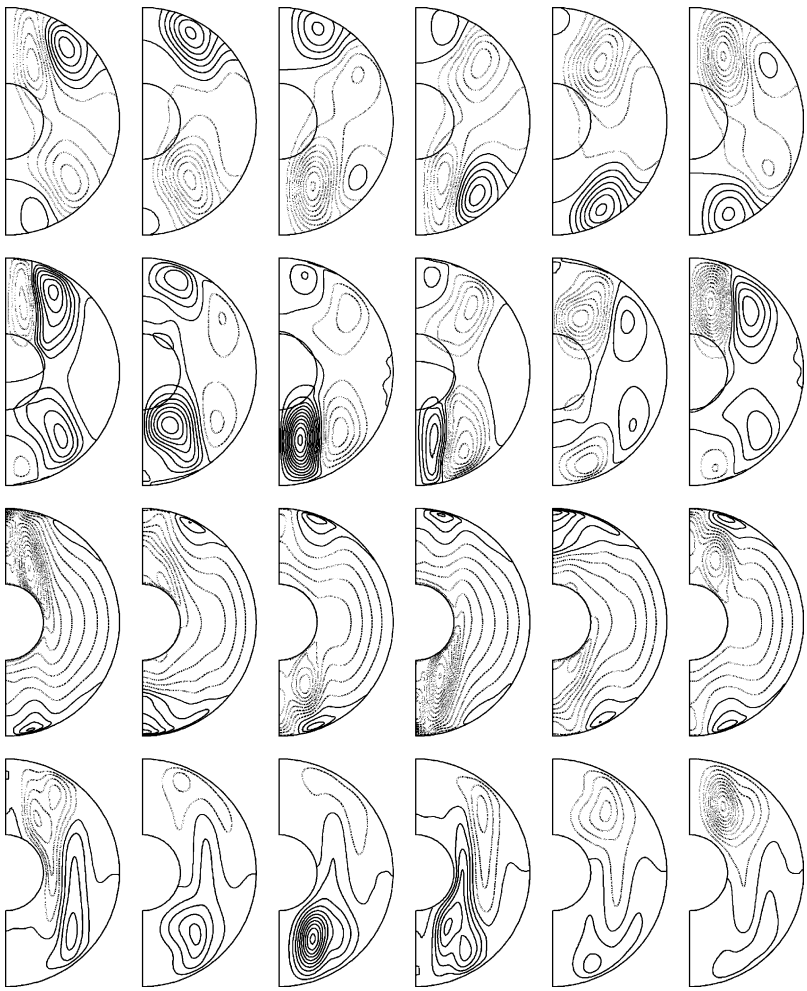

Fig. 4. Contour plots of (from top to bottom) $Ar\sin\theta$, B, $v/r\sin\theta$ and $\psi r\sin\theta$ at six evenly spaced points throughout one period at $\alpha_0 = 14.0$, $\Theta_0 = 200$. Contour intervals are 0.05, 0.5, 25 and 0.25, respectively.

The $\alpha\omega$ model was much more sensitive to the value of the time-step used than the α^2 model. For the lower range of α_0, between 6.3 and 25, Δt typically varied between 4×10^{-5} and 1×10^{-5}. In the strong field regime, above $\alpha_0 = 42$, the required time-step was 1×10^{-6} for numerical stability. In all cases, the maximum time-step that could be successfully implemented without numerical instability was used.

4.2. Linear stability results

Matters are now a little more complicated than for the α^2 dynamo since the basic states we will be testing are neither steady nor necessarily of pure parity. Previously, we were able to store the values of $\boldsymbol{B}_0$ and $\boldsymbol{u}_0$ at the collocation points and solve for the exponential behaviour of the single azimuthal mode by time-stepping Eqs. (11a) and (11b). It is certainly possible to attempt a similar approach and store the values of $\boldsymbol{B}_0$ and $\boldsymbol{u}_0$ at each collocation point over a sequence of snapshots of the periodic solution. While this approach is just as quick as before, the downside is the large memory requirements for the storage (∼100 Mb). To avoid this problem we solved the equivalent linearised 2.5D problem where the axisymmetric basic state is also solved for, but does not receive any back reaction from

the non-axisymmetric mode. This increases the CPU time requirements, but not even by a factor two since there are no $\sin(m\phi)$ parts to solve for in the axisymmetric case.

After the symmetry breaking bifurcation, both the dipole and quadrupole non-axisymmetric perturbations must grow or decay at the same rate since they are no longer independent of one another. Of course, the oscillatory nature of the underlying basic state modifies what we mean by the phrase "growth rate". The non-axisymmetric perturbations will now, in general, exhibit some sort of unknown time dependence in addition to that of the exponential growth or decay that we are trying to ascertain. This additional time dependence has the same period as the axisymmetric basic state and so a quantitative measure of the growth rate is then still possible as long as one compares values at intervals given by the period of the axisymmetric basic state.

It turns out that the pure parity quadrupole branch is stable to all non-axisymmetric perturbations up to and including $m = 8$. The eigenfunctions take the form of azimuthally drifting waves again, albeit modified by the periodic time dependence induced by the underlying basic state. At $\alpha_0 = 10.0$, just before the symmetry breaking bifurcation, the period-averaged Elsasser number, $\Lambda = 28.3$. This is identical to the value at which the first non-axisymmetric mode started growing ($m = 3$) for the α^2 dynamo and so this particular $\alpha\omega$ model appears to be more stable. However, the period-averaged energetic Elsasser number, Λ' is only 1.40 in contrast to 4.53 previously which highlights the problem of how best to define this quantity.

During the short sequence of four bifurcations which introduces dipole symmetry to the basic state the $m = 1$ decay rate is very close to marginal but is never positive. The decay rate of the $m = 1$ mode rises again immediately after the last bifurcation but begins to decrease gradually as α_0 is then increased. The decay rate for this mode is approximately 10 times smaller than for the next least stable mode, $m = 2$, and indeed it is the first mode to go unstable. The value of α_0 for marginal stability is 12.8 which corresponds to an Elsasser number of 61.2, or equivalently, $\Lambda' = 1.94$.

Compared with the α^2 dynamo, we have non-axisymmetric modes becoming unstable at much higher Λ, but much lower Λ'. The discrepancy between the values of Λ and Λ' is easily enough explained by looking again at the plots in Fig. 4. Although, at first glance, the field does not seem to be nearly as localised as for the α^2 dynamo, one must remember to take into account the fact that this is now a mixed parity solution. For the snapshots where the field is concentrated in one hemisphere there is almost no field at all in the other. Since the energetic Elsasser number involves the integral over the whole meridional section it is not surprising that it is appreciably lower than the classical Elsasser number which is based on the maximum field strength.

The obvious question now is what difference has the differential rotation made to our results. If we go by the classical Elsasser number, we conclude that instability has been inhibited, whereas, if we go with the energetic Elsasser number we could equally well say that the instability has been enhanced! It is probably the case that the ideal measure of field strength is somewhere between the two definitions given here. If we compare our results to previous work then we would expect that the differential rotation supplied here, with $\mathrm{d}\Omega/\mathrm{d}s$ predominantly greater than zero, would stabilise the system. If that is the case then it would appear that the classical Elsasser number would, in fact, be the more appropriate measure. However, the perturbation to the thermal wind that lies inside the tangent cylinder does provide a region of negative shear for some parts of the period and so perhaps Λ' is really the better choice. We will return to this issue later when we change the value of Θ_0, thus giving us something better to compare the present results with.

Fig. 5 shows the three components of the magnetic field of the $m = 1$ mode at $\alpha_0 = 14.0$ at the same evenly spaced points as for the corresponding axisymmetric plot in Fig. 4. The steady drift of the solution has been compensated for as has the growth rate. This confirms that the eigenfunction shares the same period as the basic state. Also, it has another feature in common, namely the "phase-shifted" equatorial symmetry, arising from the particular combination of even and odd harmonics in time.

During the cycle, the field is totally confined to one hemisphere, the location changing every half period. This is in agreement with the corresponding slices shown in Fig. 4 which show a similar effect but not to the same degree. One difference is that the field is located almost exclusively inside the tangent cylinder

Fig. 5. Contour plots of (from top to bottom) B_r, B_θ, and B_ϕ of the $m = 1$ eigenfunction at $\alpha_0 = 14.0$, $\Theta_0 = 200$. The slices shown are at constant ϕ after removing the steady drift component. The plots from left to right correspond exactly to those in Fig. 4. Contour intervals are the same for all plots.

for the entire period. Surprisingly though, the concentration is apparently out of phase with the $m = 0$ part. It seems then that the introduction of time dependence to the basic state allows the solution to evolve without the instability necessarily concentrating around the region of highest field strength. This differs from our previous steady state results and indeed was not observed in the work of HF, nor the magnetostrophic analyses of McLean and Fearn (1999).

4.3. Fully 3D results

Since no other values of m became unstable after the $m = 1$ mode in the range of α_0 tested, we simply obtained our initial non-axisymmetric state by using the $m = 0$ periodic solution and the $m = 1$ eigenfunction alone. As before, the linear eigenfunction, chosen at a random point in time, was given one tenth of the energy of the corresponding axisymmetric part and then time-stepped to equilibrium. This was carried out at $\alpha_0 = 13.0$ using nine azimuthal modes in addition to the axisymmetric part.

After a few diffusion timescales the solution settled in to a state with periodic axisymmetric part. The period was 0.18, which was unchanged from the purely axisymmetric case, although the time evolution of the spectral coefficients and the inner core rotation rate throughout one period was noticeably different. The non-axisymmetric parts had the same periodicity as $m = 0$ in addition to their azimuthal drift. Using this state as an initial condition, the code was then run at $\alpha_0 = 12.7$, i.e. in the regime of linear stability. After four timescales, the non-axisymmetric parts began decaying rapidly and after a further timescale they had disappeared to such an extent that the axisymmetric part had almost returned to its original unperturbed state. As with the α^2 dynamo, the initial azimuthal symmetry breaking bifurcation is supercritical.

The behaviour of the full non-axisymmetric solution in the supercritical regime is different to that of the α^2 dynamo in that the $m = 0$ mode is affected much more by the non-axisymmetric modes just after onset. This is indicated by the sequence of six snapshots of the axisymmetric part of the full solution in Fig. 6.

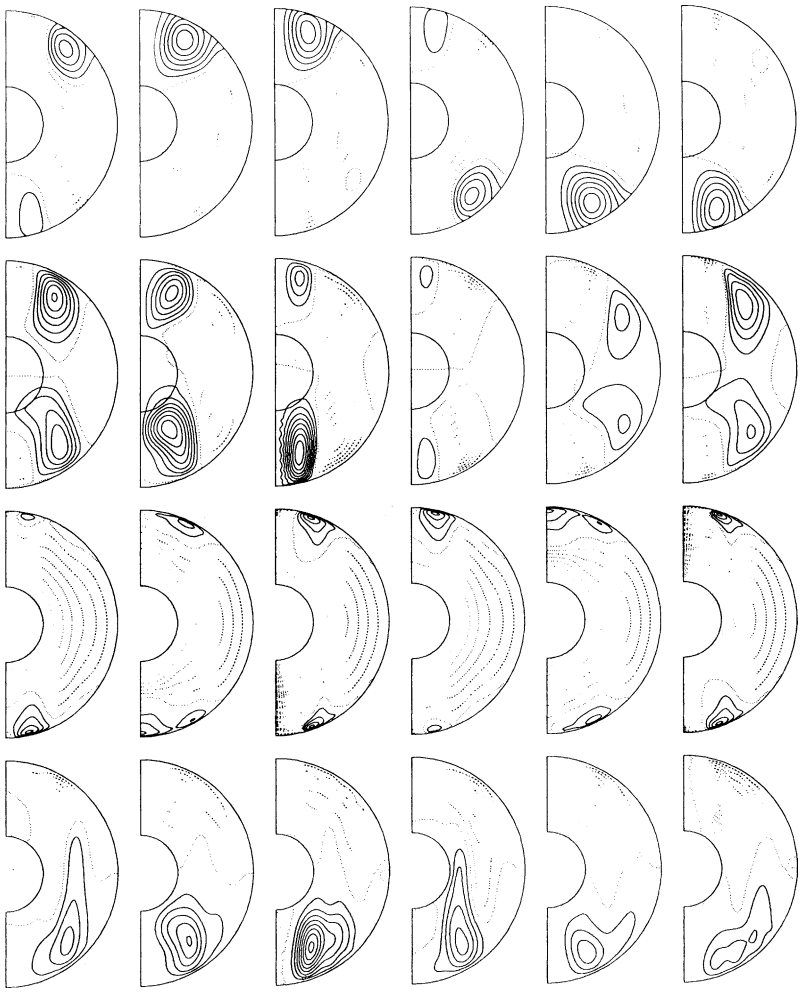

Fig. 6. Contour plots of (from top to bottom) $Ar\sin\theta$, B, $v/r\sin\theta$ and $\psi r\sin\theta$ at six evenly spaced points throughout one period of the full non-axisymmetric solution at $\alpha_0 = 14.0$, $\Theta_0 = 200$. Contour intervals are 0.05, 0.5, 25 and 0.25, respectively.

The snapshots have been chosen to coincide as closely as possible with those in Fig. 4. Although the field evolution is very similar, there are clearly some minor differences, in contrast to the equivalent set of plots for the α^2 dynamo. The flow seems to be affected to a greater extent, in particular the toroidal part. Table 7 shows how the energy decreases by roughly a factor 10 for each step in m for the large scale azimuthal modes at $\alpha_0 = 14.0$. The $m = 0$ energy has decreased by approximately 6% of its original value, 15.2.

One very noticeable feature in the $m = 1$ behaviour is the drastic change in its drift frequency, -6.79, from the linear regime, -223. The drift is still retrograde but of a much smaller magnitude. Presumably this must be directly related to the presence and non-linear interaction of all the higher m modes. If so, then this highlights how misleading a simple linear analysis can be, since the modes above $m = 1$ contribute less than 1% to the total energy of the solution. Accounting for the drift, the three components of the $m = 1$ part of the equilibrated solution are shown in Fig. 7. Compared with the linear counterpart in Fig. 5 one can see that the exact details of the mode have changed considerably, although the broad behaviour is similar.

The α^2 and $\alpha\omega$ models are also similar in the way they behave at higher forcings. With the azimuthal

Table 7
Period-averaged magnetic energies for the individual azimuthal modes at $\alpha_0 = 14.0$

m	E_M
0	14.3
1	1.08
2	0.115
3	1.60×10^{-2}
4	2.53×10^{-3}
5	5.41×10^{-4}
6	1.24×10^{-4}
7	3.22×10^{-5}
8	9.68×10^{-6}
9	4.48×10^{-6}

symmetry completely broken, the next bifurcation is to a quasi-periodic state at $\alpha_0 \sim 15$. The short period is still roughly one fifth of a timescale and is modulated by a longer period of about 0.7. The non-axisymmetric parts are also quasi-periodic as well as maintaining their azimuthal drift. There are certainly variations on the short timescale of the $m = 0$ part, but there is a clear periodic behaviour for all modes on the 0.7 timescale. This is weakly modulated by an even longer timescale, ~4, resulting in the quasi-periodicity mentioned. For $m = 1$, the drift frequency is essentially unchanged from that before the bifurcation.

5. $\Theta_0 = 400$ ($\alpha\omega$)

5.1. Axisymmetric results

We now double the buoyancy force to examine the effect of increasing the magnitude of the differential rotation. As expected, the quadrupole is still easiest to excite, but with $\alpha_c = 3.00$, which is not exactly one half of the previous value, 6.3. The discrepancy shows that, even though it is very weak, the meridional circulation can still produce an observable effect, albeit of little consequence. Similarly, for the dipole branch, the value of α_c was found to be 3.85, in contrast with 8.0 previously.

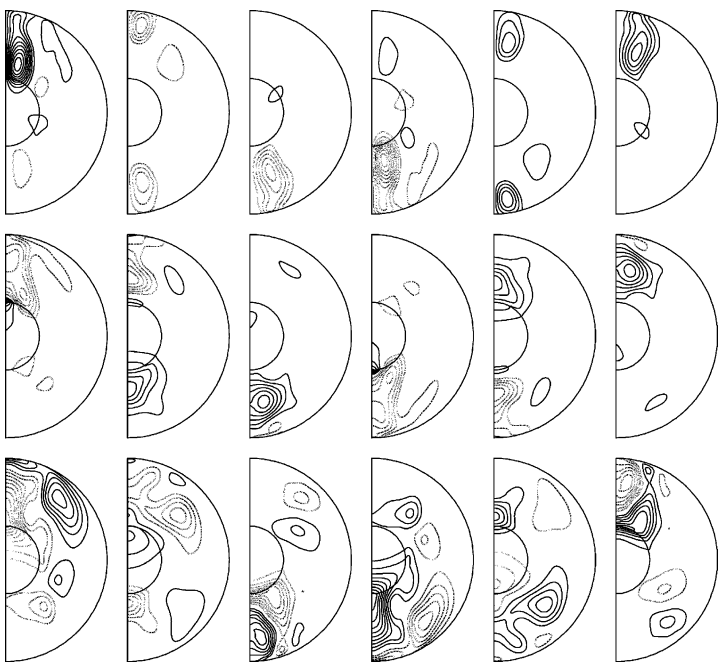

Fig. 7. Contour plots of (from top to bottom) B_r, B_θ, and B_ϕ of the $m = 1$ part of the non-axisymmetric solution at $\alpha_0 = 14.0$, $\Theta_0 = 200$. The slices shown are at constant ϕ after removing the steady drift component. The plots from left to right correspond exactly to those in Fig. 5. The contour interval is 0.2 throughout.

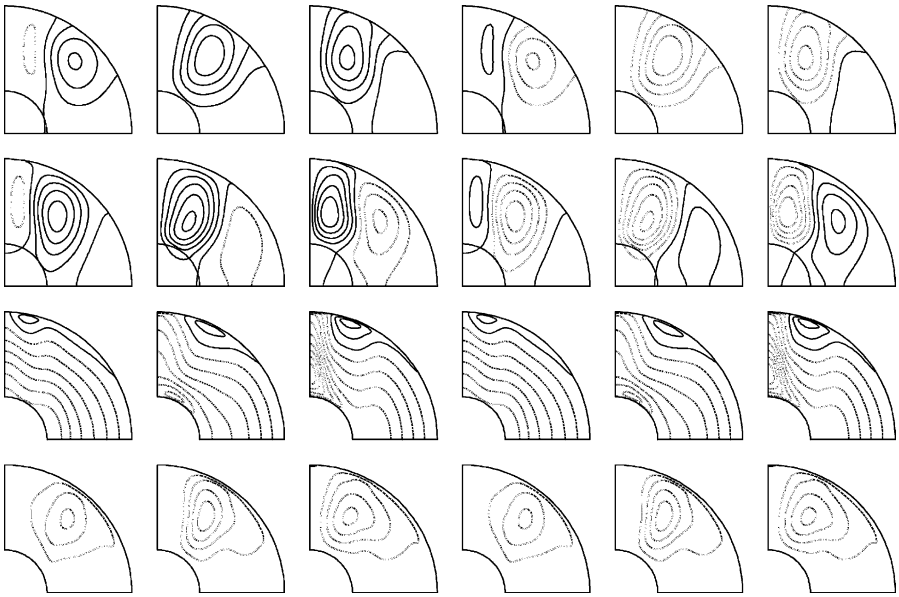

Fig. 8. Contour plots of (from top to bottom) $Ar\sin\theta$, B, $v/r\sin\theta$ and $\psi r\sin\theta$ at six evenly spaced points throughout one period at $\alpha_0 = 4.4$, $\Theta_0 = 400$. Contour intervals are 0.05, 1.0, 50 and 0.25, respectively.

The solution in the non-linear regime, past α_c, again takes on the form of an oscillatory quadrupole with zero time average. The evolution of the pure parity state throughout one period is shown in Fig. 8 at $\alpha_0 = 4.4$. This solution persists until a symmetry breaking bifurcation at $\alpha_0 = 4.5$.

The mixed parity solution which results does, however, differ from that in the last section, since the dipole part now oscillates with the same frequency as the quadrupole. It turns out that the total energy has half the period of the field, a feature shared with the flow. This implies that we have a state which only includes the odd harmonics in *both* parities. The evolution of this state throughout one period is shown in Fig. 9 at $\alpha_0 = 5.0$.

The value of α_0 for which the symmetry breaking bifurcation takes place is less than half of that for the previous model. Looking at the magnetic energy, we see that this has actually increased to 22.4 from the previous model's value of 13.7, showing that, if anything, the present model has actually had its symmetry broken later than the previous model.

The truncations for this model were increased from the last section to take into account the larger differential rotation now present. A truncation test was carried out at $\alpha_0 = 5.0$ which suggests that the field and flow should still be resolved to the same extent.

5.2. Linear results

The $m = 1$ mode was the first to go unstable at $\alpha_0 = 4.31$, which is still in the pure quadrupole regime for the basic state. Only the dipole parity was excited, although the quadrupole comes in straight after, at $\alpha_0 = 4.32$. This is slightly surprising, since the parity of the associated flow eigenfunction is dipole, which is at variance with the results of HF and for our own α^2 dynamo. Again, as we pointed out for the case of eigenfunction concentration, one may point to the time dependence as a possible candidate for disrupting the previous pattern of results. Of course, one should remember that there is not much difference between the onset of the two parities, and indeed, both are present soon afterwards when the basic state becomes mixed.

The period-averaged critical Elsasser numbers corresponding to $\alpha_0 = 4.31$ are $\Lambda = 30.9$ and $\Lambda' = 2.67$. Increasing the differential rotation has produced another situation where Λ exhibits a different change than Λ'. Since the axisymmetric plots have

Fig. 9. Contour plots of (from top to bottom) $Ar \sin\theta$, B, $v/r \sin\theta$ and $\psi r \sin\theta$ at six evenly spaced points throughout one period at $\alpha_0 = 5.0$, $\Theta_0 = 400$. Contour intervals are 0.05, 1.0, 50 and 0.25, respectively.

a quadrupole symmetry, they are even less localised than they were before, hence Λ and Λ' are closer than for the previous buoyancy. Since the positive gradient of differential rotation should be stabilising, we expect to see higher Elsasser numbers than before. It would therefore appear that the energetic Elsasser number is the appropriate measure, as expected from the differing degrees of localisation of the two basic states under comparison.

The decay rates at $\alpha_0 = 4.31$ are shown in Table 8.

Table 8
The decay rates for the pure parity eigenfunctions, obtained by comparing the solutions one period apart, at $\alpha_0 = 4.31$, $\Theta_0 = 400$

m	1	2	3	4	5	6	7	8
Dipole	+0.20	−64	−93	−115	−138	−160	−184	−208
Quadrupole	−0.39	−56	−82	−99	−125	−142	−170	−187

From these values, we can see that the $m = 1$ mode actually behaves in the opposite manner to all the others with respect to parity selection. This suggests that the preference of a dipolar flow, as opposed to the expected quadrupole, may indeed be a non-generic result, perhaps simply an artifact of our particular choice of α and Θ.

One can show easily enough that for a basic state with odd field harmonics and even flow harmonics, the resulting perturbation equations will admit two separate time dependences in the eigenfunctions. The one that is selected in this case is that having the same behaviour as the basic state, i.e. odd field and even flow. Due to its equatorial symmetries, this eigenfunction cannot localise itself within one hemisphere as with the mixed parity solution for the previous choice of Θ_0. It does, however, show signs of growth and decay throughout its periodic cycle and again is concentrated primarily within the tangent cylinder.

In the mixed parity regime, at $\alpha_0 = 5.0$, the $m = 1$ eigenfunction that grows most quickly is the one which has the opposite time dependence to the basic state. The field has even harmonics and has half the period of the flow which has the odd harmonics. Since the second half of one period will be identical to the first, Fig. 10 shows six evenly spaced snapshots of the magnetic field over the first half of the period. The relaxation of equatorial symmetry has again encouraged the solution to localise in one hemisphere, although the effect is not as pronounced as before. The localisation within the tangent cylinder still appears to be a general feature of the non-axisymmetric eigenfunctions.

5.3. Fully 3D results

A snapshot of the mixed parity $m = 1$ eigenfunction at $\alpha_0 = 5.0$ was given one tenth of the energy of the simultaneous $m = 0$ basic state and then the full non-axisymmetric equations were time-stepped forward. The solution settled in to a state with the time dependence as predicted from the linear theory. In contrast to the previous choice of Θ_0, the drift frequency of the $m = 1$ mode, -0.70 was relatively unchanged from that of the linear eigenfunction, -0.88.

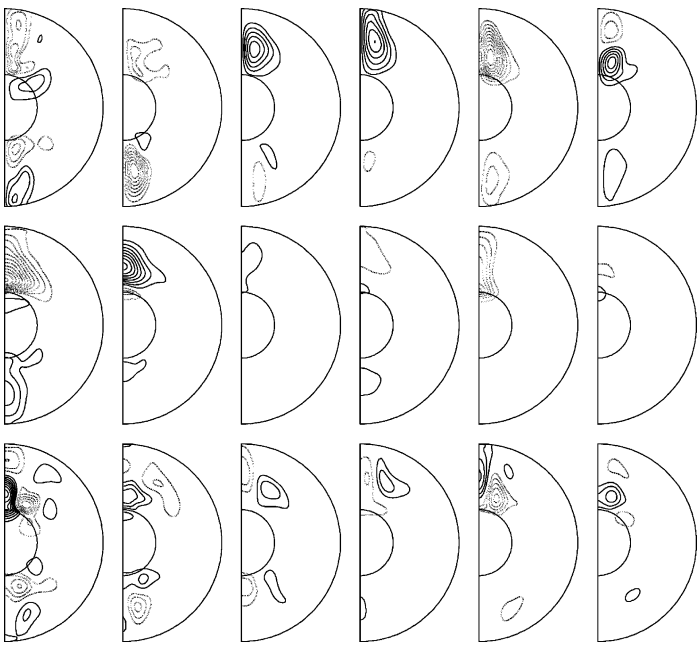

Fig. 10. Contour plots of (from top to bottom) b_r, b_θ, and b_ϕ of the $m = 1$ eigenfunction at $\alpha_0 = 5.0$, $\Theta_0 = 400$. The slices shown are at constant ϕ after removing the steady drift component and exponential growth. The first, third and fifth columns correspond exactly to the first three columns in Fig. 9. Contour interval for b_r is one half of that for the other two components.

A run was made at $\alpha_0 = 4.5$, which eventually equilibrated with finite amplitude in both symmetries and so the non-axisymmetric solution is mixed parity over at least the range indicated by the linear analysis. The next run was made at $\alpha_0 = 4.35$ in which the non-axisymmetric quadrupole and axisymmetric dipole parities began to decay. No sign of equilibration was found and so the energy in the decaying $m = 0$ dipole mode was quartered and the run restarted. This was repeated twice with no sign of the decay stopping, and so it appears that the non-axisymmetric solution follows the parity selection from the linear analysis.

A run at $\alpha_0 = 4.3$ showed immediate decay of all non-axisymmetric parts and so the procedure of reducing the energies was again employed to save time. The non-axisymmetric energies were all reduced by a factor of 25, after which they continued to decay, leading us to conclude that the azimuthal symmetry breaking bifurcation is supercritical in nature.

Returning to the structure of the non-axisymmetric solutions, we have chosen to focus on the mixed parity regime at $\alpha_0 = 5.0$. Fig. 11 shows the axisymmetric part of the solution at a sequence of similar snapshots to those in Fig. 9. The field is relatively unchanged with the flow being affected only slightly more. The

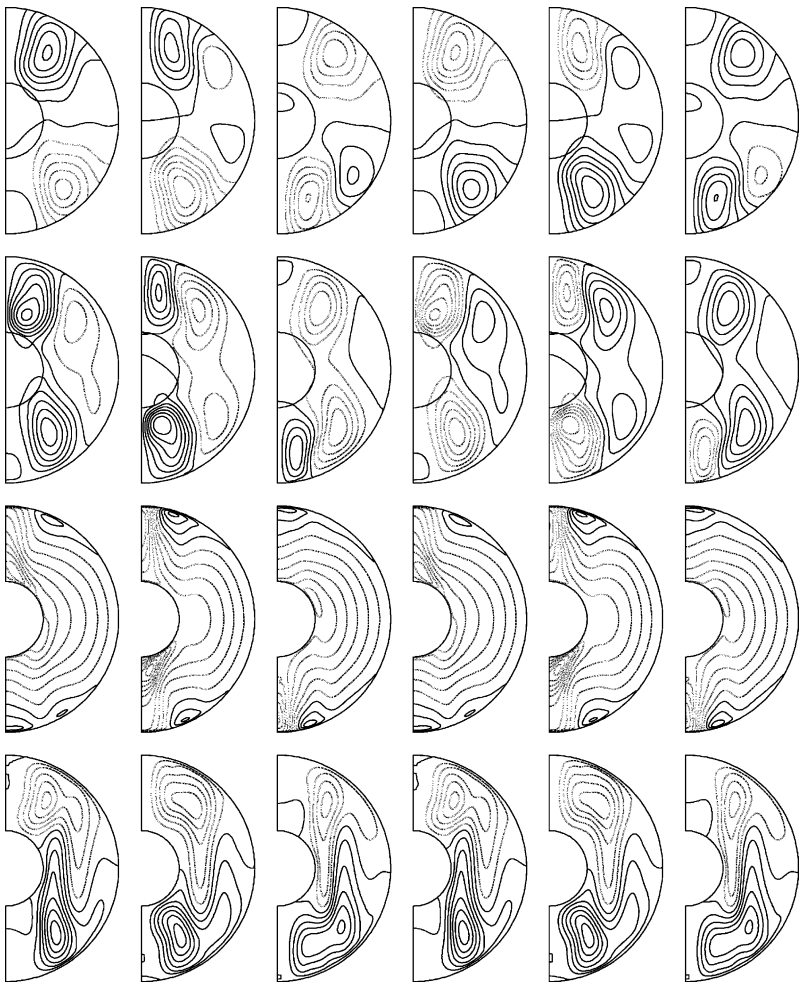

Fig. 11. Contour plots of (from top to bottom) $Ar\sin\theta$, B, $v/r\sin\theta$ and $\psi r\sin\theta$ at six evenly spaced points throughout one period of the full non-axisymmetric solution at $\alpha_0 = 5.0$, $\Theta_0 = 400$. Contour intervals are 0.05, 1.0, 50 and 0.25, respectively.

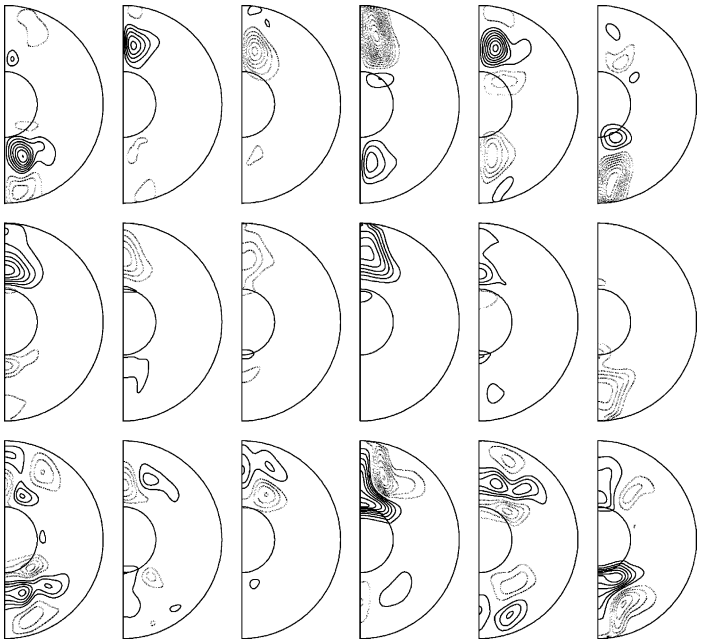

Fig. 12. Contour plots of (from top to bottom) b_r, b_θ, and b_ϕ of the $m = 1$ part of the non-axisymmetric solution at $\alpha_0 = 5.0$, $\Theta_0 = 400$. The slices shown are at constant ϕ after removing the steady drift component and exponential growth. The first, third and fifth columns correspond exactly to the first three columns in Fig. 9. Contour interval for b_r is 0.1 with 0.2 for b_θ and b_ϕ.

$m = 1$ part of the solution is shown in Fig. 12, again only over the first half of the period. As before, there seem to be a lot of fluctuations throughout a single period, but the main feature is still that the field is localised within the tangent cylinder.

6. $\Theta_0 = -200$ ($\alpha\omega$)

6.1. Axisymmetric results

The final model we shall consider is one where the direction of the buoyancy, and hence the thermal wind, has been reversed. Changing the sign of the buoyancy means we have changed the sign of the dynamo number, and so we should not necessarily expect to obtain the same values of α_c as for $\Theta_0 = +200$. One should note though that Roberts (1972) does mention a possible link between the values of α_c for opposite parities on flipping the sign of the dynamo number. Indeed, we do follow the trend exhibited by previous models in that the reversed differential rotation promotes dipole instability before quadrupole. The critical onset of the dipole mode is at $\alpha_c = 6.15$, whereas for the quadrupole it is $\alpha_c = 7.70$.

In the weakly non-linear regime the dipole solution takes the familiar form of dynamo waves oscillating about a zero mean. As expected, these waves now travel in the opposite direction to before, i.e. pole to equator. The evolution throughout one period at $\alpha_0 = 10.0$ can be seen in Fig. 13 where it should be noted that, except for the differential rotation, the contour intervals are now one half of those in the corresponding situation for $\Theta_0 = +200$ shown in Fig. 13. The probable explanation is found by inspection of the angular velocity, which now shows a greater region of opposite flux than its earlier counterpart, thus limiting the toroidal field, and, in turn, the meridional field.

At $\alpha_0 = 11.2$, the dipole branch becomes unstable. However, the subsequent evolution is completely different than for the negative buoyancy. Instead of undergoing a symmetry breaking bifurcation, the solution jumps to a separate pure parity quadrupole

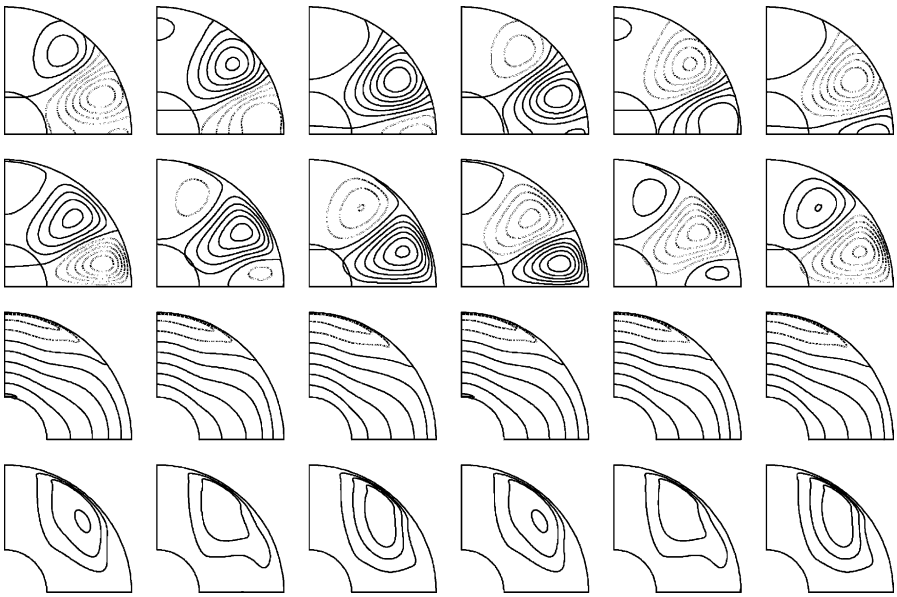

Fig. 13. Contour plots of (from top to bottom) $Ar\sin\theta$, B, $v/r\sin\theta$ and $\psi r\sin\theta$ at six evenly spaced points throughout one period at $\alpha_0 = 10.0$, $\Theta_0 = -200$. Contour intervals are 0.025, 0.25, 25 and 0.125, respectively.

branch. Using this solution as an initial condition, it was possible to return to $\alpha_0 = 10.7$ before losing stability back to the dipole branch. It is possible that we have actually found a subcritical bifurcation, even though it is not in the manner originally envisaged! The dipole branch may undergo a subcritical bifurcation, presumably to an unstable mixed parity solution, which then bifurcates to the pure quadrupole branch, regaining stability in the process. This type of situation could be potentially very important in the context of geomagnetic reversals in which the predominantly dipolar field can become quadrupolar during the reversal process. If a perturbation to the long-term dipole field causes it to flip to the quadrupole state, then the removal of the perturbation may cause it to flip back to either the original state or, equally possibly, the reversed state. The quadrupole state observed here has lower energy than the dipole, which also fits the data from reversals. The quadrupole state is very similar to the dipole and can be seen in Fig. 14 for $\alpha_0 = 12.0$. All the field is still virtually contained outside the inner core and the presence of only the odd harmonics in time induces a flow with half the period.

The equatorial symmetry is eventually broken at $\alpha_0 = 12.5$ to a state that contains only odd harmonics in both dipole and quadrupole parts. For $\Theta_0 = +200$, the sequence of mixed solutions contained a quadrupole part with energy essentially independent of α_0, corresponding to the energy of the pure parity state prior to the bifurcation. Here, for $\Theta_0 = -200$, we also observe growth of the dipole energy alone as α_0 is increased although the quadrupole energy is not equal to that before the bifurcation. This is outlined in Fig. 15 which shows the quadrupole contribution to the energy as bullet points. At the point of bifurcation, the energy is distributed evenly between the two parities suggesting an equipartition of energy. This does not persist as α_0 is increased though, with the dipole part increasing linearly with α_0.

From Fig. 15, we see that that global period-averaged magnetic energy of the solution at $\alpha_0 = 16.0$ is only 5.54, compared to 17.7 at the equivalent value of α_0 for the opposite buoyancy. It seems that the differing behaviour of the toroidal flow between the two cases is responsible for the difference. To underline this, the period-averaged energy for $\alpha_0 = 30.0$ is still only 13.8. It is evident that in

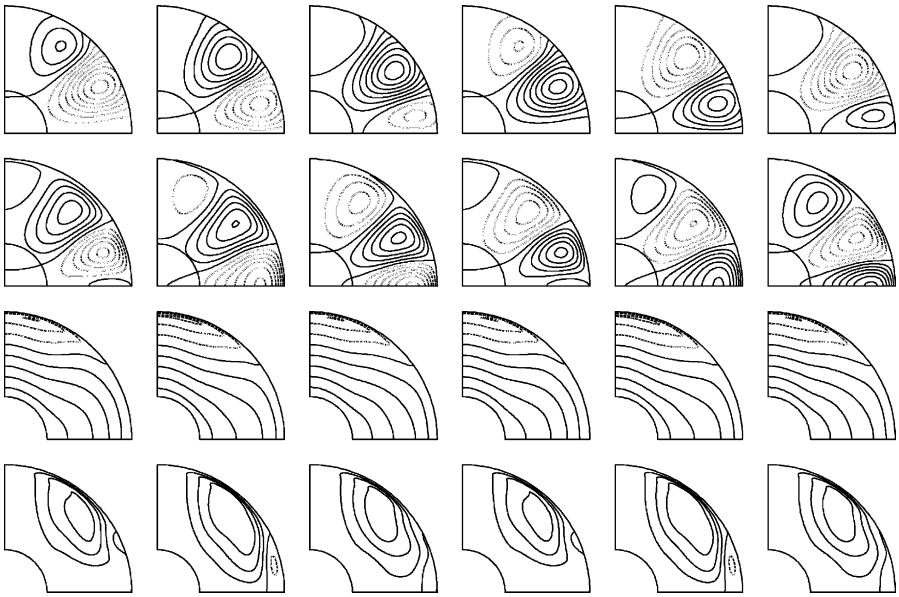

Fig. 14. Contour plots of (from top to bottom) $Ar\sin\theta$, B, $v/r\sin\theta$ and $\psi r\sin\theta$ at six evenly spaced points throughout one period at $\alpha_0 = 12.0$, $\Theta_0 = -200$. Contour intervals are 0.025, 0.25, 25 and 0.125, respectively.

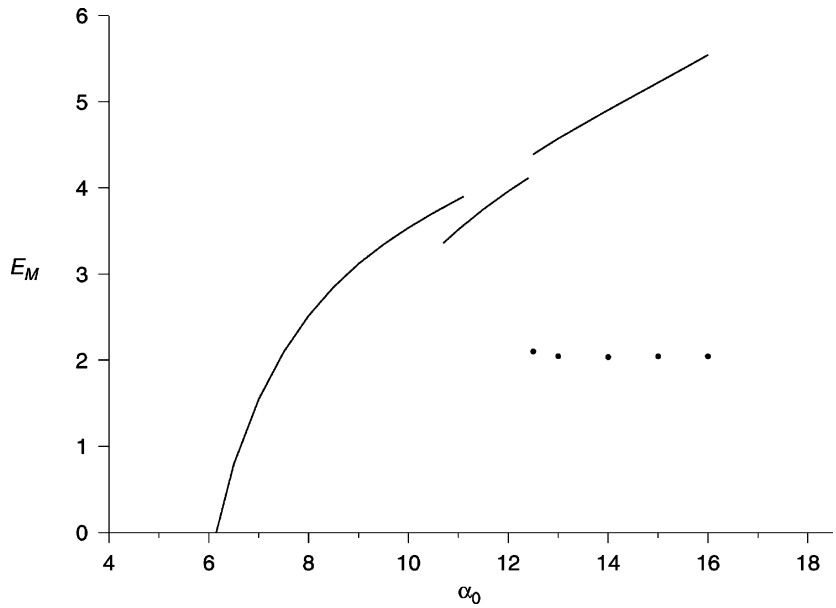

Fig. 15. E_M vs. α_0 for $\Theta_0 = -200$. The quadrupole contribution to the energy in the mixed regime is shown by bullet points.

this regime, increasing α_0 has little effect on the (still dominant) toroidal field. The interaction of magnetic and thermal winds is pushing the system away from the strong field regime towards the weak field regime where poloidal and toroidal parts are comparable.

That the magnetic wind opposes the thermal wind in this case, and not for the other, is not surprising in the weakly non-linear limit. We know that, despite the linear eigenfunctions having different parities, the overall structure is usually very similar and so the generated magnetic wind should therefore be similar. What we have shown here is that this similarity can persist into the strongly non-linear regime and thereby change the evolution of the two systems entirely as α_0 is increased.

6.2. Linear results

A linear analysis was made which revealed that no modes were unstable at $\alpha_0 = 30.0$, although $m = 1$ was the least stable. At $\alpha_0 = 64.0$, the period-averaged energy is ∼49 and a truncation test was carried out which revealed no serious problems. Despite the high energy present in the basic state, no instabilities were found. It was not until $\alpha_0 \sim 75$ that instability was observed, and even then not in the manner expected. The modes that showed growth were with azimuthal wavenumbers of order 10 with the lower modes coming in gradually as α_0 was increased. At $\alpha_0 \sim 120$, the $m = 1$ mode eventually became unstable but a lack of time unfortunately prevented a full analysis of the situation. Since the truncation test shows no problem at $\alpha_0 = 64.0$, it would appear these results are genuine, but one would like to be definite given the strange behaviour observed. Clearly, a fully 3D run is out of the question since we would have to include an extremely large number of azimuthal modes to be able to resolve the fine structures which would inevitably appear.

7. Conclusions

The first aim of the study was to examine the magnitude of axisymmetric field one must have in a spherical geometry in order to obtain non-axisymmetric instabilities. Table 9 summarises the critical parameter values associated with the onset of the first non-axisymmetric mode.

Table 9
Critical parameter values for the four different models attempted

	Θ_0			
	0	+200	+400	−200
α_0	13.1	12.8	4.31	∼75
m	3	1	1	O(10)
E_M	32.0	13.73	18.9	∼61
Λ	28.3	61.2	30.9	∼41
Λ'	4.53	1.94	2.67	∼8.6

From a general point of view it would seem that instability typically ensues when $\Lambda \sim O(10)$ and when $\Lambda' \sim O(1)$. This agrees with the work of Zhang and Fearn (1994, 1995) who studied the instabilities of imposed toroidal and poloidal decay modes separately. When there is a non-zero buoyancy Λ_c is slightly higher although Λ'_c is actually lower. It is difficult to reconcile the results with and without the buoyancy term, but one must bear in mind that the two models differ fundamentally in that one is steady state (as was the Zhang and Fearn work) and one is oscillatory. It would appear that the time dependence can produce noticeably different results. The non-axisymmetric instabilities produced by the oscillatory states always showed a tendency to concentrate within the tangent cylinder, while the steady state field filled the whole shell.

If we compare the $\Theta_0 = 200$ solution with the one having twice the buoyancy, we can make a better comparison. There is less localisation in the $\Theta_0 = 400$ solution and so Λ decreases leaving us with Λ' as the more appropriate measure. The effect of doubling the predominantly positive gradient differential rotation, is to stabilise the system as previously noted by Ogden and Fearn (1995).

For the case where $\Theta_0 = -200$ the interaction of the thermal wind and the magnetic wind unfortunately produced a flow of little interest with respect to the study of negative gradient differential rotation. Inside the tangent cylinder, the gradient of the angular velocity with respect to the cylindrical radius is quite small, however, near the equator there are regions of negative gradient differential rotation. Given the tendency of all our oscillatory solutions

to have their instabilities concentrated within the tangent cylinder region it is perhaps not surprising that the expected behaviour was not found. The negative gradient regions disappear completely for higher forcings which helps to explain why the onset of instability is found at such large values of α_0 and Λ'.

Another issue raised by Zhang and Fearn was the direction of propagation of the instabilities. It was their conclusion that this quantity could be strongly influenced by small effects like changing the inner core radius slightly or even simply small changes in the basic state field. For the α^2 model the $m = 3$ mode propagates eastward, but we only ever obtain westward propagating waves when the buoyancy is included. It is difficult to say without studying more models, but it may be the case that the introduction of time dependence favours westward drifting modes. This could have important implications for the geomagnetic field, which is known to have a westwardly drifting non-axisymmetric component (see for example, Bloxham and Gubbins, 1985).

The second aim of our study was to examine the possibility of subcritical solutions at the point of azimuthal symmetry breaking. Regardless of whether the basic state was steady or oscillatory there was no evidence for subcriticality in any of the models studied. We did, however, find evidence of a subcritical axisymmetric bifurcation in our last model. This bifurcation allows a dipole solution to temporarily change to a weakened quadrupole state, with the possibility of returning to a reversed dipole solution. This may be more relevant than the bifurcations we were originally trying to find.

Lastly, we also looked at how the instabilities could affect the basic state once they were allowed to evolve and equilibrate at finite amplitude. In all cases, the basic state did not undergo any radical change but it was clear that the instabilities were able to draw more energy in the oscillatory solutions than for the steady state. This may be related to the fact that the α^2 model produced an $m = 3$ instability first rather than the $m = 1$ mode of the other models. For the oscillatory models, the azimuthal dependence of the whole solution within the core was not just dominated by $m = 0$ and $m = 1$ but by some of the higher modes as well. This is unlikely to be observed at the Earth's surface, however, since there was virtually no penetration of our non-axisymmetric fields into the mantle.

Acknowledgements

Paul Fotheringham would like to thank EPSRC for the funding of this work through a studentship.

References

Alfe, D., Kresse, G., Gillan, M.J., 2000. Structure and dynamics of liquid iron under Earth's core conditions. Phys. Rev. B 61, 132–142.

Bloxham, J., Gubbins, D., 1985. The secular variation of the Earth's magnetic field. Nature 317, 777–781.

Fearn, D.R., 1983. Hydromagnetic waves in a differentially rotating annulus. I. A test of local stability analysis. Geophys. Astrophys. Fluid Dyn. 27, 137–162.

Fearn, D.R., 1984. Hydromagnetic waves in a differentially rotating annulus. II. Resistive instabilities. Geophys. Astrophys. Fluid Dyn. 30, 227–239.

Fearn, D.R., 1985. Hydromagnetic waves in a differentially rotating annulus. III. The effect of an axial field. Geophys. Astrophys. Fluid Dyn. 33, 185–197.

Fearn, D.R., 1988. Hydromagnetic waves in a differentially rotating annulus. IV. Insulating boundaries. Geophys. Astrophys. Fluid Dyn. 44, 55–75.

Fearn, D.R., Lamb, C.J., McLean, D.R., Ogden, R.R., 1997. The influence of differential rotation on magnetic instability and non-linear magnetic instability in the magnetostrophic limit. Geophys. Astrophys. Fluid Dyn. 86, 173–200.

Hollerbach, R., 2000. A spectral solution of the magneto-convection equations in spherical geometry. Int. J Numer. Meth. Fl. 32, 773–797.

Hollerbach, R., Glatzmaier, G.A., 1998. Mixed-parity solutions in a mean-field dynamo model. Stud. Geophys. Geodyn. 42, 239–246.

Hollerbach, R., Jones, C.A., 1993. A geodynamo model incorporating a finitely conducting inner core. Phys. Earth Planet. Int. 75, 317–327.

Hutcheson, K.A., Fearn, D.R., 1995. The non-linear evolution of magnetic instabilities in a rapidly rotating annulus. J. Fluid Mech. 291, 343–368.

Hutcheson, K.A., Fearn, D.R., 1996. The stability of toroidal magnetic fields with equatorial symmetry: implications for the Earth's magnetic field. Phys. Earth Planet. Int. 97, 43–54.

Hutcheson, K.A., Fearn, D.R., 1997. The stability of toroidal magnetic fields with equatorial symmetry: evolution of instabilities. Phys. Earth Planet. Int. 99, 19–32.

Levy, E.H., 1972. Kinematic reversal schemes for the geomagnetic dipole. Astrophys. J. 171, 635–642.

McLean, D.R., 1997. Ph.D. Thesis, University of Glasgow.

McLean, D.R., Fearn, D.R., 1999. The geostrophic nonlinearity and its effect on magnetic stability. Geophys. Astrophys. Fluid Dyn. 90, 79–112.

Ogden, R.R., Fearn, D.R., 1995. The destabilising nature of differential rotation. Geophys. Astrophys. Fluid Dyn. 81, 215–232.

Parker, E.N., 1969. The occasional reversal of the geomagnetic field. Astrophys. J. 158, 815–827.

Roberts, P.H., 1972. Kinematic dynamo models. Phil. Trans. R. Soc. Lond. A 272, 663–703.

Zhang, K., Fearn, D.R., 1994. Hydromagnetic waves in rapidly rotating spherical shells generated by magnetic toroidal decay modes. Geophys. Astrophys. Fluid Dyn. 77, 133–157.

Zhang, K., Fearn, D.R., 1995. Hydromagnetic waves in rapidly rotating spherical shells generated by poloidal decay modes. Geophys. Astrophys. Fluid Dyn. 81, 193–209.